EXAFS studies of $SrSn_{1-x}Sb_xO_3$ and $BaPb_{1-x}Bi_xO_3$

Wendy R. Flavell,*[a] Michael Mian,[a] Adam J. Roberts,[b]† Julian F. Howlett,[a] Md. Moinuddin Sarker,[b]‡ Paul L. Wincott,[c] Robert L. Bilsborrow[d] and Gert van Dorssen[d]

[a]*Department of Physics, UMIST, PO Box 88, Manchester, UK M60 1QD*
[b]*Department of Chemistry, UMIST, PO Box 88, Manchester, UK M60 1QD*
[c]*Department of Chemistry/IRCSS, University of Manchester, UK M13 9PL*
[d]*CLRC Daresbury Laboratory, Daresbury, Warrington, Cheshire, UK WA4 4AD*

EXAFS is used to study changes in local structure which occur on doping at the B site in two related perovskite oxides, $SrSn_{1-x}Sb_xO_3$ and $BaPb_{1-x}Bi_xO_3$. In the case of the stannate, data is taken at the Sr K, Sb K and Sn K edges. A combination of near-edge XAS and EXAFS measurements show that Sb dopes into the material as Sb^V. In the case of the bismuthate, data is taken at the low-intensity Bi L_I and Pb L_{II} edges, with the aim of resolving controversy surrounding the interpretation of EXAFS data taken at the overlapping L_{III} edges. In $BaBiO_3$, two Bi—O bond lengths are observed, suggesting the presence of a charge density wave. In this material, equal proportions of these two bond lengths are present. However, as Pb is doped into the material, the proportion of oxygen bonded to Bi at the shorter of the two distances increases progressively.

The electronic structure of complex perovskite metal oxides is of considerable interest, as the properties of these oxides may be tailored to specific applications by subtle changes in chemical doping, particularly at the B cation site in the general formula ABO_3. Here we describe results from two systems, $SrSn_{1-x}Sb_xO_3$ and its row 6 analogue $BaPb_{1-x}Bi_xO_3$. The former is of interest as a potential catalyst for partial oxidation of hydrocarbons[1] (unusual in a perovskite, as these are normally good deep oxidation catalysts), while the latter is a high-temperature oxide superconductor in the composition range $0.05 \leqslant x \leqslant 0.3$, with a maximum T_c of *ca.* 13 K at $x = 0.25$.[2] The system undergoes a metal-to-non-metal transition to a charge density wave semiconductor at $x \approx 0.4$.[3] In contrast, $SrSnO_3$ is a wide bandgap insulator. When Sb is doped into the material, the introduced electrons appear to be compensated (possibly by metal vacancy formation), so that a transition to a metallic state is not achieved.[4,5] This contrasts with the behaviour of the electronically related material, $Sn_{1-x}Sb_xO_2$.[6]

In order to complement a programme of electronic structure investigation,[4,7,8] stations 7.1 and 9.2 at the SRS, CLRC Daresbury Laboratory have been used to obtain information from EXAFS about the variation in local coordination as the dopant is introduced. This is combined with information from near-edge XAS, allowing us to infer the valence states of the B metal cations in the bulk material.

Experimental

Preparation of samples and data collection

Ceramic samples of both systems were prepared using high-temperature solid-state routes, involving firing intimately ground stoichiometric mixtures of Bi_2O_3 (99.99%), PbO (Analar) and $BaCO_3$ (Analar) for $BaPb_{1-x}Bi_xO_3$, and $SrCO_3$ (99%), SnO_2 (99.9%) and Sb_2O_3 (99.9%) for $SrSn_{1-x}Sb_xO_3$. In the case of the latter, the procedure developed by Cava *et al.*[9] was adopted to minimise volatilisation of the Sb dopant.[4]

All powder samples were characterised by XRD and SEM–EDAX. In the case of $BaPb_{1-x}Bi_xO_3$, which is known to form a complete solid solution from $x = 0$ to $x = 1$, no trace of any secondary phase was observed in XRD, and the Bi:Pb ratio in all samples was consistent with the bulk nominal doping level, within the limits of accuracy of the EDAX technique. In contrast, samples of $SrSn_{1-x}Sb_xO_3$ were single-phase only within the composition range $0 \leqslant x \leqslant 0.085$ (for samples annealed at the same final synthesis temperature of 1360 °C), and for $x \geqslant 0.1$, peaks due to an $SrSb_2O_5$ secondary phase were evident in XRD. Our EXAFS measurements were therefore concentrated on the doping range below the bulk solubility limit at $x \approx 0.085$. In this respect, the stannate system is similar to $Sn_{1-x}Sb_xO_2$, in displaying a rather low tolerance to Sb doping.[6]

XAS data were recorded on stations 7.1 and 9.2 at the SRS, CLRC Daresbury Laboratory. The SRS ran at 2 GeV, with a typical beam current of 230 mA. In the case of $SrSn_{1-x}Sb_xO_3$, EXAFS data were recorded at the Sn K, Sb K and Sr K edges, whilst near-edge information was obtained at the softer Sn and Sb L_{III} edges. In the case of the $BaPb_{1-x}Bi_xO_3$ system, data were taken at the weak L_I edge of Bi and L_{II} edge of Pb, in an attempt to resolve controversy surrounding the interpretation of EXAFS data from the strongly overlapping L_{III} edges of Bi and Pb.[10,11] Whilst the separation of the L_{III} edges is only 364 eV, the separations of the L_I and L_{II} edges are 527 eV and 511 eV, respectively. The choice of the L_I edge for the heavier element (Bi) and the L_{II} edge for the lighter element (Pb) minimises the contributions of absorption from one element to the EXAFS of the other. However, a penalty is incurred in terms of the signal-to-noise ratio, as both edges are considerably weaker than the respective L_{III} edge. The effects of this on data analysis, and on the information which may be extracted reliably, are discussed below.

Measurements of the Sn L_{III}, Sb L_{III}, Pb L_{II} and Bi L_I edges were made in transmission mode, using the order-sorting double-crystal Si(111) monochromator on station 7.1. Measurements of the Sr K and Sn K edges were made in transmission mode, using the order-sorting double-crystal Si(220) monochromator on line 9.2. Measurements of the Sb K edge at 30.5 keV necessitated the use of an Si(220) channel-cut monochromator. The low Sb doping levels of the $SrSnO_3$ samples required the use of fluorescence detection, using the liquid-nitrogen-cooled Canberra Mk II 13-element solid-state detector on line 9.2.

---

† Current address: Leverhulme Centre for Innovative Catalysis, Department of Chemistry, University of Liverpool, Liverpool, UK L69 3BX.

‡ Current address: Institute of Atomic and Molecular Sciences, Academia Sinica, PO Box 23–166, Taipei, Taiwan 106, ROC.

For each set of measurements, appropriate standard spectra were recorded. These were particularly useful in analysing valence state information from near-edge data. The standards used for $SrSn_{1-x}Sb_xO_3$ were SnO (99+%, Sn^{II}), SnO_2 (99.995%, Sn^{IV}), Sb_2O_3 (99.9%, Sb^{III}) and Sb_2O_5 (99.995%, Sb^{V}). The use of SnO as a standard for Sn^{II} was treated with caution as it is known that it is oxidised readily in air at room temperature,[12] and as a result may contain a significant fraction of Sn^{IV}. For $BaPb_{1-x}Bi_xO_3$, the standards used were PbO_2 (99.999%, Pb^{IV}), PbO (Analar, Pb^{II}) and Bi_2O_3 (99.99%, Bi^{III}). It is difficult to obtain Bi^{V} in a pure form. Commercially supplied $NaBiO_3$ is known to be at best only 80–90% pure, with significant contamination from Bi^{III} phases.[13] We therefore used two Bi^{V} standards, commercially obtained $NaBiO_3$ (80–90%), and Li_3BiO_4, a relatively stable Bi^{V} compound which was prepared freshly by reaction of Li_2O (97%) with Bi_2O_3 (99.99%) under O_2 in accordance with the procedure of Greaves and Katib.[14]

Samples for XAS were ground intimately with BN diluent, packed uniformly into the window of an aluminium sample holder, and held in place between two pieces of Sellotape. Measurements were made at room temperature. Near-edge data only were recorded at the Sn L_{III} and Sb L_{III} edges. EXAFS data were recorded to $k_{max} = 15$ Å^{-1} for the Sr K, Sn K and Sb K edges of $SrSn_{1-x}Sb_xO_3$. For the weak Pb L_{II} and Bi L_I edges of $BaPb_{1-x}Bi_xO_3$, the spectra were recorded to $k_{max} = 12$ Å^{-1}.

EXAFS data analysis

Raw data were corrected for dark currents and converted to $\boldsymbol{k}$-space, summed and background subtracted to yield the EXAFS function $\chi(\boldsymbol{k})$ using the EXCALIB and EXBACK programs.[15] A k^3 weighting function was used to enlarge the oscillations at high $\boldsymbol{k}$. In the case of the Sr K and Sn K edges of $SrSn_{1-x}Sb_xO_3$, the oscillations in $\chi(\boldsymbol{k})$ were extremely strong, and clear oscillations were visible to 15 Å^{-1}. For the Sb K edge, oscillations were weaker (owing to the dilute nature of the samples), and for analysis purposes the data were truncated at 11.5 Å^{-1}. The Pb L_{II} and Bi L_I edges were very weak, and as a result showed significant noise beyond *ca.* 8–10 Å^{-1}.

The Daresbury Laboratory EXCURV92 program[16] was used to fit model $k^3\chi(\boldsymbol{k})$ curves to the experimental data. Phase-shift corrections were calculated using Xalpha exchange and ground-state potentials. Sr K, Sn K and Sb K edge data were of a high quality, and as a result, no Fourier filtering was used in the data analysis. However, the weak oscillations observed at the Bi L_I and particularly the Pb L_{II} edge, together with the fact that the Bi L_I edge lies only 527 eV above Pb L_I, meant that only first-shell information could be extracted from the data reliably. The data was thus Fourier filtered to extract the k^3-weighted contribution from the first oxygen shell surrounding the Bi and Pb absorbers, and a fit was obtained to this information. The spectra were Fourier transformed in a Gaussian window with a width of 0.1 Å. To allow for the possibility of the absorbing atoms occupying more than one site, the calculation of $\chi(\boldsymbol{k})$ was modified by the inclusion of a factor G_s, representing the fraction of absorbing atoms at a particular site, defined such that

$$\sum_{s=1}^{n} G_s = 1 \qquad (1)$$

where n is the number of different sites. Thus the EXAFS modulation is given by:

$$\chi(\boldsymbol{k}) = \sum_j \frac{G_s N_j}{k r_j^2} S_i(\boldsymbol{k}) F_j(\boldsymbol{k}) \exp(-2\sigma_j^2 k^2) \times \exp[-2r_j/\lambda_j(\boldsymbol{k})] \sin[2kr_j + \phi_{ij}(\boldsymbol{k})] \qquad (2)$$

where $F_j(\boldsymbol{k})$ is the back-scattering amplitude from each of the N_j neighbouring atoms of the jth type with a Debye–Waller factor of σ_j at a distance r_j away from the absorber. ϕ_{ij} is the total phase shift experienced by the photoelectron, λ_j is the electron mean-free-path length, and $S_i(\boldsymbol{k})$ is the amplitude reduction factor due to many-body effects.

During iteration of the fitting parameters, care was taken to avoid correlation effects between those parameters that are related strongly to the EXAFS amplitude (the Debye–Waller factor, the coordination number and the amplitude reduction factor), and between those which affect the frequency of the EXAFS oscillations (the coordination distance and the threshold position). Particular difficulties were encountered in obtaining physically reasonable coordination numbers in multi-shell analyses such as that used for the stannate. This problem originates in the very low scattering strength from oxygen compared with the heavy cations within the structure. In multi-shell EXAFS data, coordination numbers are often constrained to a value near the ideal for the model structure. In the present case, the coordination numbers were iterated independently, and omitted from the final iteration of all parameters simultaneously. This method is a slight improvement on complete constraint to an ideal coordination number, in that the fit to the data is improved, whilst retaining a number which makes chemical sense. Estimated errors are included in Table 1.

Results and Discussion

$SrSn_{1-x}Sb_xO_3$

Data from two separate structural determinations for $SrSnO_3$ were used to provide the model data for a fit to the K edge EXAFS data. In the first of these, Megaw proposed an ideal undistorted cubic perovskite structure as shown in Fig. 1(a).[17] The more recent work of Vegas *et al.*, using a combination of electron diffraction and X-ray diffraction, gives the distorted structure shown in Fig. 1(b).[18] Attempts were made to fit the EXAFS data to both models. However, it was found that a reasonable fit to the experimental EXAFS of $SrSnO_3$ could be obtained only by assuming the distorted perovskite structure (of space group *Pbnm*) determined by Vegas *et al.*[18] This suggests that the more recent structural determination[18] is likely to be correct, and also illustrates that the EXAFS data is remarkably sensitive to small structural distortions. A comparison between the bond lengths obtained from XRD[18] and from Sn K edge EXAFS is shown in Table 1. No attempt was made to fit the second oxygen shell from the absorber, as the scattering from this light ion at large distances gave an insignificant scattering amplitude in simulated data. In some cases, the exceptional quality of the data allowed the data to be fitted to back-scattering shells up to 7 Å from the absorber. However, for radial distances greater than *ca.* 4 Å, the effects of multiple scattering may become significant.[19] As the fit to the EXAFS data is made within the single scattering approximation, little reliance is placed on the fit to distances larger than this. With these provisos, Table 1 shows that the information from EXAFS is in good agreement with XRD of $SrSnO_3$,[18] with the major discrepancies being in coordination numbers, as discussed above.

Having obtained a good fit to the undoped parent material, $SrSnO_3$, data from the Sn K, Sb K and Sr K edges of the doped samples were fitted. Fig. 2 shows the Sn K edge $k^3\chi(\boldsymbol{k})$ EXAFS and its transform over the single-phase doping range for samples annealed at 1360 °C. Comparable data for the Sb K edge are shown in Fig. 3, while Fig. 4 shows a representative Sr K edge. The bond length information resulting from fitting these data is given in Fig. 5. Good fits to the data could only be obtained by assuming that Sb dopes onto the Sn sites in the lattice. The most significant gross change to the radial distributions on doping is seen in the contribution of next-nearest-neighbour Sr to the Sn K edge data shown in Fig. 2.

Table 1 Local radial distribution and coordination number about the central Sn atom determined for $SrSnO_3$ from Sn K edge EXAFS and XRD[18]

	EXAFS[a]			XRD[c]	
atom	radius/Å	coord. no.	DW factor	radius/Å	coord. no.
O	2.025 ± 0.002	4.5 ± 0.3	0.003	2.054–2.066	6
Sr	3.398 ± 0.008	3.0 ± 0.9	0.010	3.436–3.552	8
Sr	3.542 ± 0.009	2.9 ± 1.0	0.011		
Sn	4.063 ± 0.004	4.4 ± 1.1	0.011	4.032–4.035	6
O	—[b]	—[b]	—[b]	4.218–5.663	30
Sn	5.631 ± 0.004	3.3 ± 1.6	0.005	5.705–5.707	12

[a] For the EXAFS analysis, that standard deviations as calculated by EXCURV92 are shown. These estimates of precision overestimate the accuracy, particularly in cases of high correlation between parameters. More realistic standard deviations for the distances are 0.01 Å for small radii, up to 0.04 Å at larger radii, and ±20% in coordination number and Debye–Waller (DW) factor. The residual index, R, given by

$$R = \left\{ \sum_{i=1}^{N} k_i^3 (\chi_i^{\text{obs}} - \chi_i^{\text{calc}})^2 \right\} \Big/ \left[\sum_{i=1}^{N} (k_i^3 \chi_i^{\text{obs}})^2 \right]$$

was calculated as 29% for the complete seven-shell fit shown in Fig. 2(a). [b] No attempt was made to fit the second oxygen shell from the absorber (see text). [c] The bond lengths from the XRD structure determination of Vegas *et al.*[18] are available as supplementary material (SUP 57192, 8 pages) from the British Library. Details are available from the Editorial Office on request.

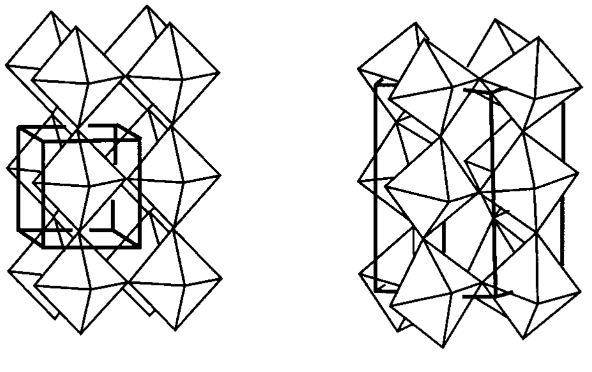
(a) (b)

Fig. 1 (a) The undistorted cubic perovskite structure (as adopted, for example, by $BaSnO_3$). (b) The distorted perovskite structure adopted by undoped $SrSnO_3$.[18]

The contribution of the Sr shell to the radial distribution is marked by an asterisk. It can be seen that as the concentration of dopant is increased, the Sr peak becomes broader and less well resolved. In the fitting process, this had the result that for $x \leqslant 0.02$, it was possible to fit two shells of Sr ions at two discrete distances from Sn, suggestive of a distorted perovskite. However, for $x > 0.02$, only one shell at an average distance between the two could be distinguished. This gives rise to the artificial discontinuity in the bond length information shown in Fig. 5(b). The corresponding Debye–Waller factor for the single Sr shell increased from *ca.* 0.01 Å^2 (for each of the two separate shells) to a typical value of 0.03 Å^2. The data suggest that the static disorder in the Sr positions (a 'soft' feature of the structure[17]) increases with doping. This is borne out by analysis of the Sr K edges (Fig. 4), where it was found that the Debye–Waller factors for each fitted shell were larger than those obtained from the Sn and Sb K edge data, and the R factors for the fit to each shell were on average 12% bigger. Typical R factors for a six or seven shell fit were in the range 25–29% for the Sn and Sb K edges, but in the region of 34–35% for the corresponding Sr K edges. Typical Debye–Waller factors of 0.01–0.015 Å^2 for the Sn/Sb edges rose to 0.02–0.03 Å^2 for the Sr K edge.

Sb—O and Sn—O distances are plotted as a function of doping level (up to the bulk solubility limit of $x = 0.085$) in Fig. 5. The Sb—O distance is considerably shorter than the Sn—O distance, and agrees well with the Sb^{V}—O distance in a number of oxides, including, for example, $K_3Sb_5O_{14}$ and $K_2Sb_4O_{11}$.[20] Unfortunately, however, it is impossible to assign unambiguously the Sb valence state in the stannate as Sb^{V} from the EXAFS data alone, as reported Sb^{III}—O distances (*e.g.* for Sb_2O_3[21]) span a very wide range, some of them below 2 Å. An assignment of Sb valence state is therefore made by combination of this data with L_{III} near-edge information discussed below. However, we note that the EXAFS data give no evidence for the presence of two different Sb—O distances, such as might be expected if the material contained mixed Sb^{III} and Sb^{V} valences. This contrasts with the behaviour obtained in the $BaBi_{1-x}Pb_xO_3$ system, where Bi is generally assumed to show mixed Bi^{III} and Bi^{V} valences, or at least some charge separation into $Bi^{4+\delta}$ and $Bi^{4-\delta}$ valences.[22] Our results for this system are presented in the next section.

As a function of doping, there appears to be a slight increase in the Sn—O distance, together with a slight decrease in the Sb—O distance, but neither is very significant in relation to the error bars. In our XRD work, we observe a very slight reduction in lattice parameter with Sb doping,[4,5] consistent with the replacement of some Sn—O bonds by shorter Sb—O distances. This is also reflected in the EXAFS data by the slight reduction in Sb—O and Sb—Sr distances with doping. The slight increase in the Sn—O distance might be consistent with a model along the lines of that suggested by Claessen *et al.* for $BaSn_{1-x}Sb_xO_3$, where distortion of the lattice of SnO_6 octahedra by the introduction of short Sb—O bonds results in a compensating enlargement of the adjacent O—Sn bond.[23] A direct comparison between the XRD lattice parameter and the EXAFS data may be made by measurement of the Sn—Sn/Sb and Sb—Sn/Sb distances (which would correspond to the lattice parameter of the simplest cubic unit cell of an undistorted perovskite). This comparison gives quite good agreement between XRD and EXAFS data.[5] However, we have not shown these data here as the distances involved are $\geqslant 4$ Å, with the result that the errors and uncertainties in the EXAFS single-scattering analysis are too large to make such a comparison strictly valid.

To complement K edge data, near-edge information from the Sn and Sb L_{III} edges was obtained, in principle giving access to the dipole-allowed transitions $2p_{3/2,1/2} \rightarrow 5s,5d$. The resulting data, together with those for the respective standards, are shown in Fig. 6 and 7, after subtraction of a linear background determined from the pre-edge region. It is immediately obvious that both the Sn and Sb XANES show considerable structure, and the assignment of peaks is not trivial. The Sb L_{III} edges of the stannate (Fig. 7) are complicated additionally by the overlap with the Sn L_{II} edge at 4156 eV. Considering first the Sn L_{III} edges, it can be seen that the XANES of the stannate samples are very similar to that of the Sn^{IV} standard, SnO_2. This might be expected as both show octahedral local coordination of Sn by O. The edge position for each compound

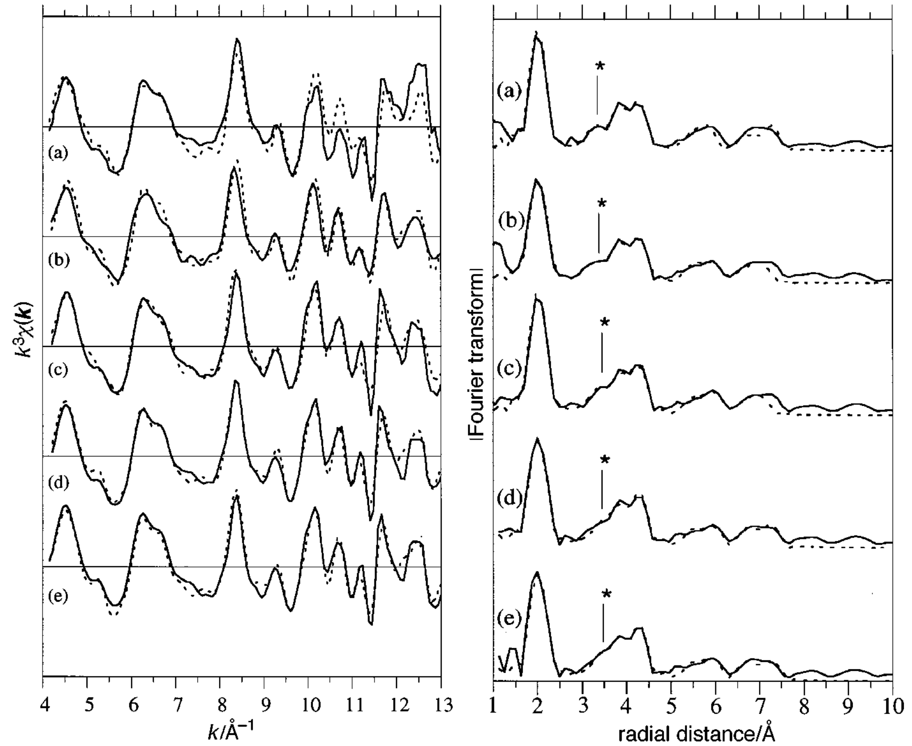

Fig. 2 $k^3\chi(k)$ and its Fourier transform for the Sn K-edge EXAFS of $SrSn_{1-x}Sb_xO_3$, (a) $x=0$; (b) $x=0.01$; (c) $x=0.02$; (d) $x=0.05$; (e) $x=0.085$. The solid line represents the experimental data; the calculated fit is shown by the dotted line. The contribution of the first Sr shell to the radial distribution lies in the region marked by asterisks.

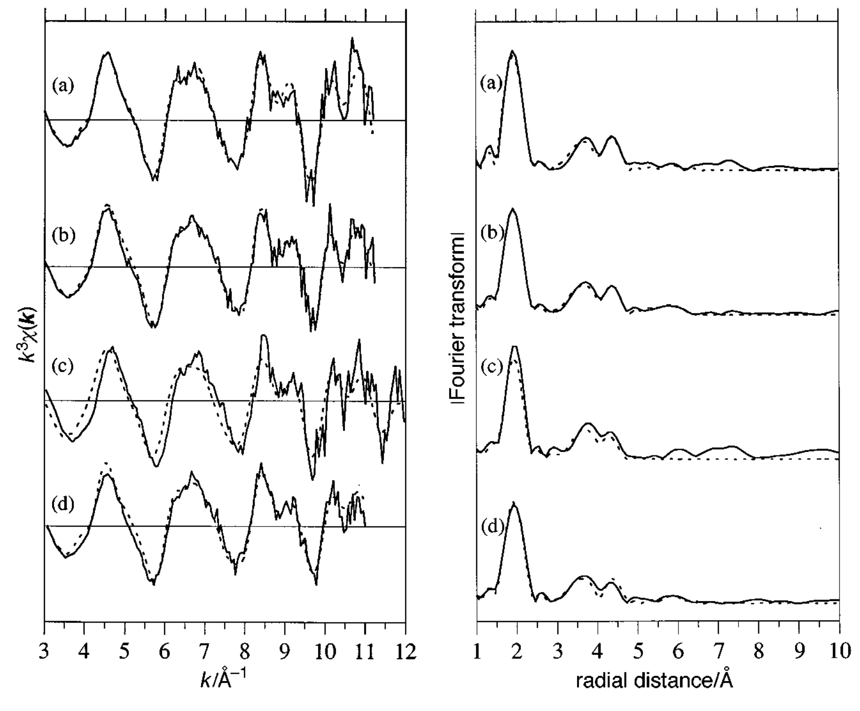

Fig. 3 $k^3\chi(k)$ and its Fourier transform for the Sb K-edge EXAFS of $SrSn_{1-x}Sb_xO_3$, (a) $x=0.085$; (b) $x=0.07$; (c) $x=0.05$; (d) $x=0.02$. The solid line represents the experimental data; the calculated fit is shown by the dotted line.

was determined from the differentiated XANES spectrum. All edge positions, including those of the standards, were found to be coincident at 3930 ± 1 eV. (The Sn L_{III} edge of elemental Sn occurs at 3929 eV.[24]) Thus, the Sn oxidation state has little effect on the position of the L_{III} absorption edge. (A similar effect is seen in XPS, where there is no Sn 3d binding energy shift between Sn^{II} and Sn^{IV}.[25]) Thus, whilst the bond length information from EXAFS [Fig. 5(a)], the stability of the material in air, and the similarity of the stannate XANES to that of SnO_2 lead us to infer a valence state of IV for Sn, the assignment of valence from the XANES itself is not unambiguous.

By analogy to the reference material, SnO_2, we expect the unfilled states above the threshold energy to be of s and p character, with the maximum in the 5d density of states above the vacuum level.[26] We assign the first absorption feature in the Sn L_{III} spectra (at *ca.* 3932 eV) to the $2p_{3/2}\rightarrow5d$ transition, rather than to the transition into 5s. This assignment is supported by a number of features of the spectra. First, the feature is seen in the XANES of both Sn^{IV} and Sn^{II} standards

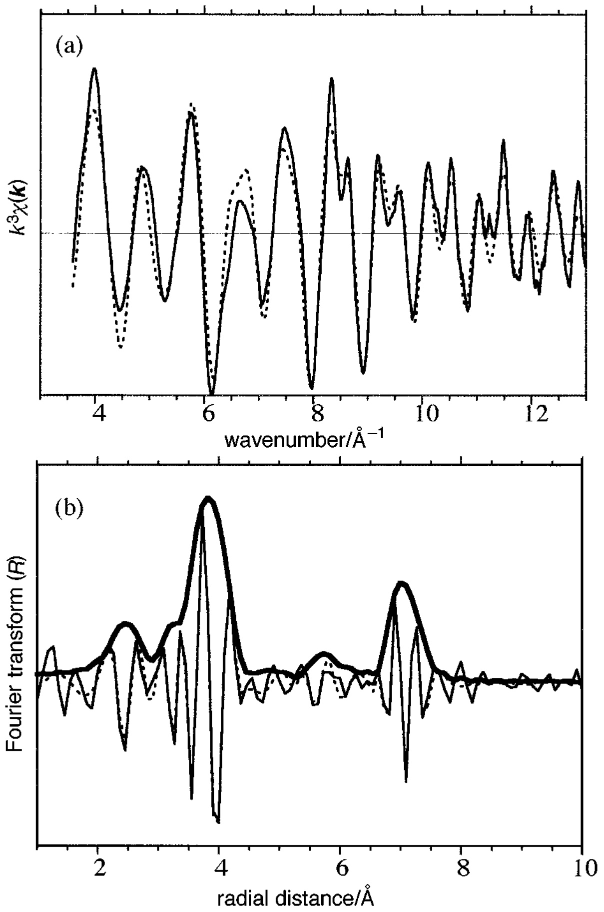

Fig. 4 Examples of the fits obtained to the Sr K-edge EXAFS data for $SrSn_{0.99}Sb_{0.01}O_3$, showing the stages of data analysis: (a) $\chi^3(k)$ *vs.* k; (b) $F(r)$ and $|F(r)|$ *vs.* r. In both cases, the dotted line represents the fit to the data (solid line), which is unfiltered.

(and there is an analogous feature in the XANES of both Sb^{III} and Sb^{V} materials, see Fig. 7). The 5s level is full in Sn^{II} and Sb^{III}, and the transition $2p_{3/2} \rightarrow 5s$ is therefore impossible. Secondly, the p→d transition is expected to dominate over p→s by a factor of 50 in polycrystalline samples.[27] On this basis, the first excitation appears to be far too strong relative to the remaining edge structure to be assigned to the transition into 5s. Furthermore, electronic structure calculations for the related material $BaSn_{1-x}Sb_xO_3$ show that the 5s density of states (DOS) above the Fermi energy, E_F, is very low.[28] Thus, it appears that Sn^{IV} and Sb^{V} L_{III} edges do not show a distinct 'pre-edge' feature associated with the unoccupied 5s levels, in marked contrast to that observed for the 6s DOS associated with Bi^{V} and Pb^{IV}.[29]

Assignment of the other near-edge features is made difficult by a lack of literature data for these edges. The L edge absorption spectra of In and Sn have been studied by Sham.[30] This author notes that in Sn, the unoccupied 4f band is sufficiently close to the Fermi level to hybridise with the s, p and d states, producing fine structure in the L_{III} edge XANES (the transition becoming allowed through df hybridisation). We note that the unoccupied f levels in the oxide would be expected to be at lower energy (closer to E_F) than in the metal, and by comparison with the work of Sham,[30] we tentatively assign the feature at *ca.* 11 eV above the threshold to a $2p_{3/2} \rightarrow 5df$ state. A shoulder to the low energy side of this feature is unassigned. We note that this is only seen in the XA spectra of the stannates. By comparison with inverse photoemission spectra[4] we suggest that this may be associated with some influence of Sr on the unoccupied Sn/O state hybridisation. Band-structure calculations of the distribution of the Sn

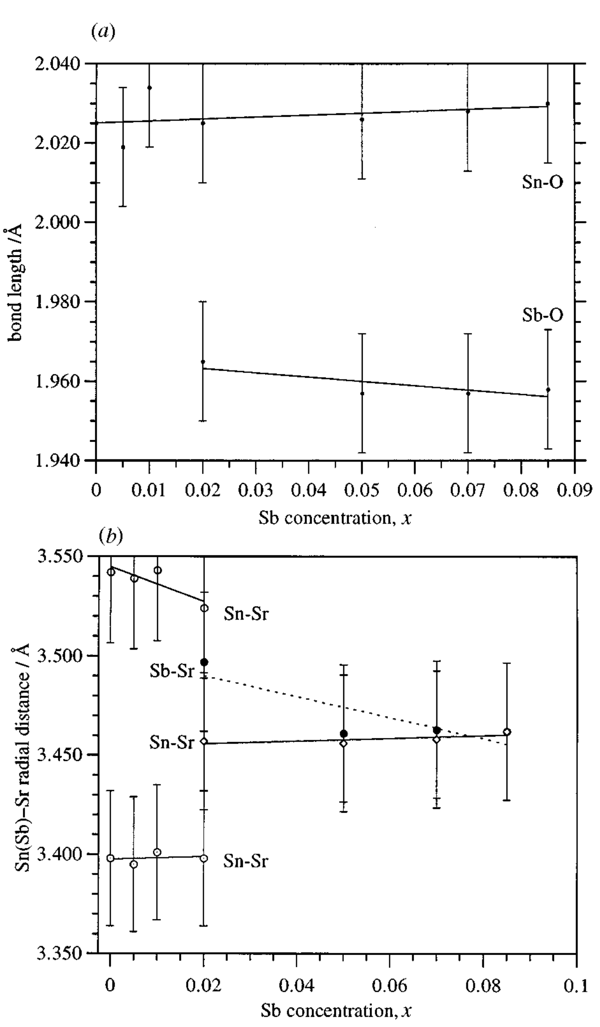

Fig. 5 Bond length information obtained from analysis of the Sb and Sn K-edges of $SrSn_{1-x}Sb_xO_3$. (a) Distances to the first O shell; (b) distances to the first Sr shell.

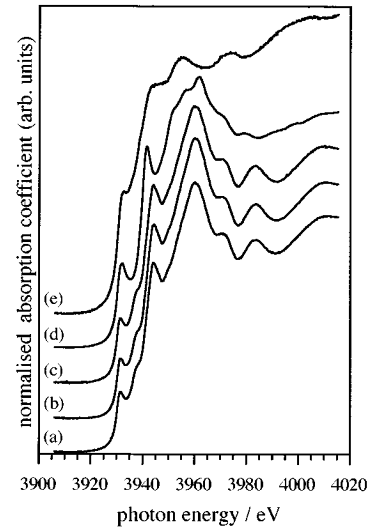

Fig. 6 Normalised Sn L_{III} XA spectra for $SrSn_{1-x}Sb_xO_3$: (a) $x=0.085$; (b) $x=0.01$; (c) $x=0$; (d) SnO_2 (Sn^{IV}); (e) SnO (Sn^{II})

unoccupied DOS in $SrSnO_3$ are necessary to assign this structure properly.

Fig. 7 shows the first 20 eV of the Sb L_{III} edge structure of the samples. Unfortunately, the later parts of the spectra are dominated by the overlapping Sn L_{II} edge at 4156 eV. Also shown are the spectra of the Sb^{III} and Sb^{V} standards. The

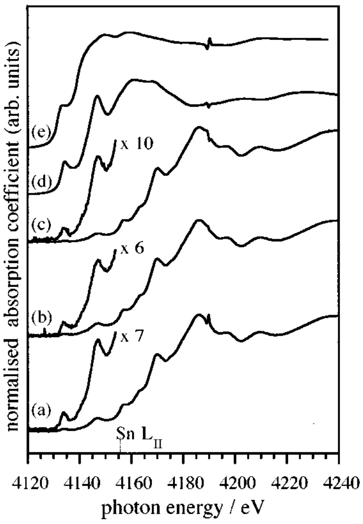

Fig. 7 Normalised XA spectra over the Sb L_{III} and Sn L_{II} near-edge region for $SrSn_{1-x}Sb_xO_3$: (a) $x=0.085$; (b) $x=0.07$; (c) $x=0.05$; (d) Sb_2O_5 (Sb^V); (e) Sb_2O_3 (Sb^{III}). The feature at 4192 eV is due to a discontinuity in monochromator output.

small feature at 4192 eV is due to miscancellation of a discontinuity in the monochromator output, which is nevertheless useful for confirming internal calibration of the scans. Close to the threshold, it is apparent that there are strong similarities between this data and the Sn L_{III} edges (Fig. 6). We follow a similar assignment, in particular assigning the first feature (present in the spectra of both the Sb^{III} and Sb^V standards) to the $2p_{3/2} \rightarrow 5d$ transition.

The edge positions were determined from the first differentials of the absorption spectra. The edges of the stannates and Sb_2O_5 are coincident at 4133 ± 1 eV, while the Sb_2O_3 edge lies at 4135 ± 1 eV. In contrast to the Sn edges, there appears to be a small but significant shift in edge position between III and V valences. (Again, a similar effect is seen in XPS, where there is an Sb 3d binding energy shift of *ca.* 1 eV between Sb^{III} and Sb^V.[23]) This, combined with the strong similarity between the stannate and Sb_2O_5 edges, and the information from EXAFS (discussed above), leads us to assign a valency of V for Sb in the doped materials.

$BaPb_{1-x}Bi_xO_3$

Fig. 8 and 9 show examples of fits obtained to the Pb L_{II} and Bi L_I edge data for the bismuthate, $BaPb_{1-x}Bi_xO_3$. As described above, because of the poor signal-to-noise level at these weak edges, we have used the data to obtain first shell information only. The raw data were Fourier filtered to extract the k^3-weighted contribution to the EXAFS from the first oxygen shell. The resulting Pb/Bi—O bond length information (R) and metal coordination number by oxygen (N) are shown in Fig. 10 and 11. Error bars are shown. As can be seen, these vary with composition, being highest for the Pb edge when $x \rightarrow 1$ (low Pb concentration), and conversely highest for the Bi edge when $x \rightarrow 0$. Data for the Pb L_{II} edge are shown in Fig. 10. It was possible here to fit the data assuming a single Pb—O bond length of *ca.* 2.15 Å. It can be seen that this distance fluctuates slightly as a function of composition, but that the variations are not very significant compared to the error bars. The coordination number is six and shows no significant variation from this as a function of composition. (The coordination number was obtained by initially fixing its value at six, while obtaining a trial fit to the data. Having achieved this, the coordination number was allowed to float both independently and, in the final stage of the analysis, together with all other parameters.) Thus the Pb edge may be fitted assuming Pb is coordinated to close to six oxygen nearest

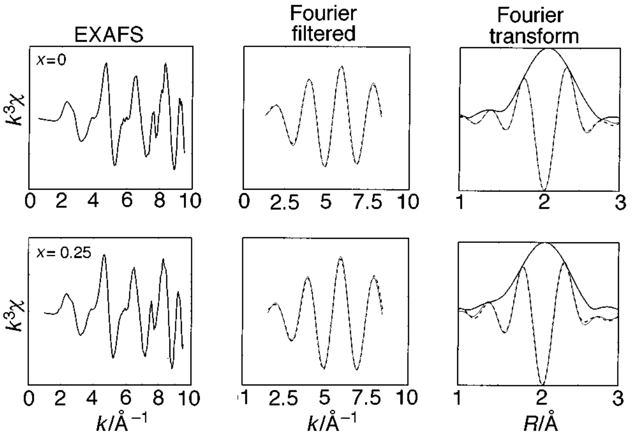

Fig. 8 An example of the Pb L_{II}-edge data, and fits to it for $BaPb_{1-x}Bi_xO_3$. The left-hand panels show raw $k^3\chi(\boldsymbol{k})$ data, while the centre panels show the results of Fourier filtering to extract the contribution from the first shell of backscatterers (see text). $F(r)$ and $|F(r)|$ *vs.* r are shown in the right-hand panels. The dashed lines show the calculated fits to the data.

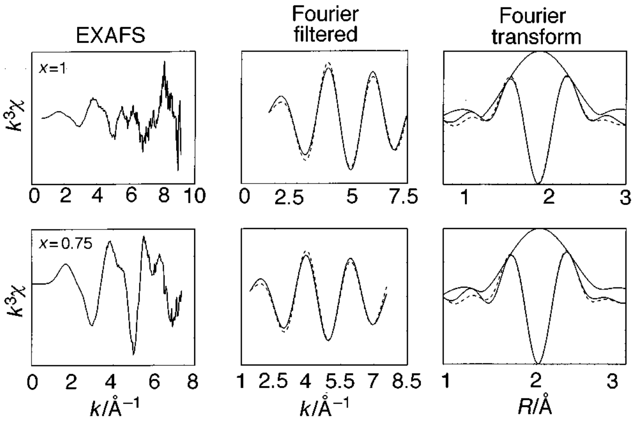

Fig. 9 An example of the Bi L_I-edge data, and fits to it for $BaPb_{1-x}Bi_xO_3$. The left-hand panels show raw $k^3\chi(\boldsymbol{k})$ data, while the centre panels show the results of Fourier filtering to extract the contribution from the first shell of backscatterers (see text). $F(r)$ and $|F(r)|$ *vs.* r are shown in the right-hand panels. The dashed lines show the calculated fits to the data.

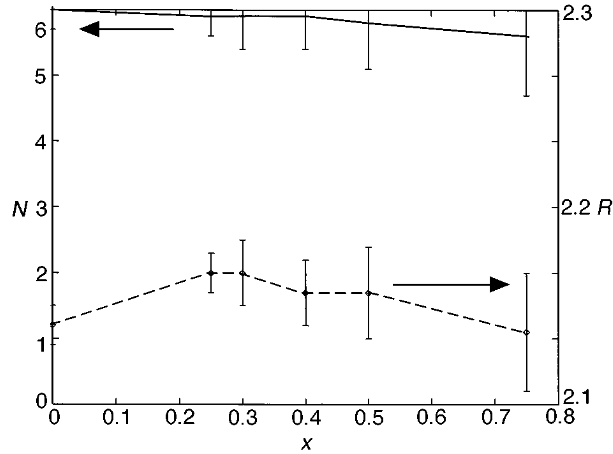

Fig. 10 Bond length and coordination number information obtained from analysis of $BaPb_{1-x}Bi_xO_3$ EXAFS; Pb—O bond length (R) and coordination number to oxygen (N), from Pb L_{II}-edge data

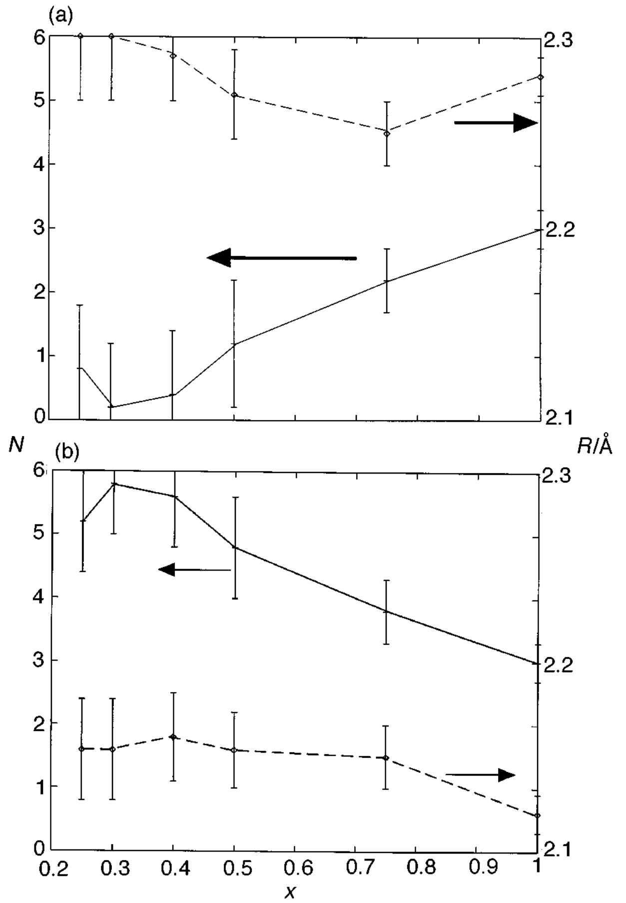

Fig. 11 Bond length and coordination number information obtained from analysis of $BaPb_{1-x}Bi_xO_3$ EXAFS; Bi—O bond lengths (*R*) and coordination numbers to oxygen (*N*), from Bi L_I-edge data. (a) Data for the longer of the two Bi—O distances; (b) data for the shorter Bi—O distance.

neighbours in a regular octahedron, across the whole composition range. The Pb—O distance is consistent with Pb in a IV oxidation state.[11] The Debye–Waller factors calculated for the O atoms around Pb were 0.04–0.06 Å^2 (±10%) for the whole composition range.

A more complex picture emerges for the oxygen coordination around Bi (Fig. 11). By comparing Fig. 10 and 11, it may be seen that the radial distribution extracted from the Fourier-filtered signal is considerably broader for the oxygen distribution around Bi than for that around Pb. This suggests strongly that the coordination of O to Bi is not as regular as in the case of Pb. Here a good fit may not be obtained for octahedral coordination; rather, two different Bi—O bond lengths are obtained, one of *ca.* 2.12–2.15 Å and a longer distance of 2.25–2.30 Å. Coordination numbers were obtained as above, initially choosing a value of three for the coordination numbers of both Bi sites for all samples, but allowing the coordination number to float at all subsequent stages of the darta analysis. In $BaBiO_3$, the average coordination number of Bi to both types of oxygen is three, so there are equal proportions of the two types of bond. The bond lengths for $BaBiO_3$ are 2.28 and 2.12 Å, in excellent agreement with the values obtained from the L_{III} edge EXAFS data of Boyce *et al.* (2.27 and 2.13 Å) and Akhtar *et al.*[11] (2.28 and 2.10 Å), and with values obtained from neutron diffraction of 2.28 and 2.12 Å by Cox and Sleight[31] and 2.26 and 2.14 Å by Thornton and Jacobson.[32] A significant difference in Debye–Waller factors between the two types of oxygen site is also observed; for the closer site, values lie in the range 0.05–0.06 Å^2 for all compositions, while for the longer distance values of 0.07–0.10 Å^2 (±10%) are found. This could be due to the greater static disorder of the more distant shell relative to Bi,[11] but is also consistent with this shell being bound less tightly to the Bi site.

Thus our data support the analysis of Boyce *et al.*[10] and other workers, in particular the observation of an irregular coordination environment for Bi.[10,33] This is consistent with observations from neutron diffraction and was assigned previously to the presence of Bi in two different average valence states, which we write as $Bi^{IV+\delta}$ and $Bi^{IV-\delta}$ (in the limit Bi^{III} and Bi^{V}).[22,31,32] This produces a distortion of the structure of $BaBiO_3$ from a simple cubic perovskite to monoclinic as a result of rotation of the BiO_6 octahedra around the pseudo-cubic [110] axis and a symmetric breathing-mode distortion produced by the oxygen atom displacements towards and away from the Bi sites.[34] This is the origin of the charge density wave behaviour of the material.[34] Whilst suggesting that there may be some disproportionation, structural techniques cannot determine the magnitude of δ directly. The system has been investigated quite extensively by XPS,[35–41] revealing some contradictory results. Although no consensus has emerged, generally only one (sometimes broadened or asymmetric) component to the Bi core level emissions has been observed. This is open to two interpretations: either δ is small, *i.e.* the charge separation is not great, or, as XPS is a highly surface-sensitive UHV technique, the surface of the material may be reduced to Bi^{III}. Indeed, Orchard *et al.* noted as early as 1977 that, unless exceptional precautions are taken in sample preparation, a mixed-valence compound may have a surface phase containing only one of the two oxidation states present in the bulk material.[35] Consistent with this, a number of authors find the majority Bi species binding energy to be close to that of Bi^{III}.[35,37,39,41] In the absence of evidence for the size of the charge separation, we describe the oxidation states as $Bi^{IV+\delta}$ and $Bi^{IV-\delta}$.

Fig. 11 shows that two different O sites remain when Pb is doped into $BaBiO_3$, in agreement with the results of Boyce *et al.*[10] Moreover, we find that the relative proportions of the two types of oxygen change as x decreases (Fig. 11). The number of O coordinated to Bi at the shorter of the two distances increases steadily with Pb doping, until it reaches 5–6 at $x=0.25$ (at a distance of 2.15 Å), while the number of O at the longer distance decreases to 0–1 (at a distance of 2.3 Å) at this point. This may offer some rationalisation of an apparent disparity between the results of Boyce *et al.*[10] and Akhtar *et al.*[11] for the Pb-doped material. The former authors find irregular coordination of Bi across the range $x=1$–0.25,[10] while the latter find regular octahedral Bi coordination (with Bi—O distance of 2.12 Å) for compositions in the range $x=$ 0.25–0.3.[11] Our results show that the population of the distant O site for $x=0.25$–0.3 is sufficiently low for its influence on the EXAFS signal to be small.

Accepting for the present the idea that the irregular coordination of Bi is associated with charge disproportionation, we associate the shorter Bi—O distance with a $Bi^{IV+\delta}$—O bond, and the longer with $Bi^{IV-\delta}$—O pairs. The observation of a significantly smaller Debye–Waller factor for the closer O site would be consistent with its assignment to the more correlated motion of a $Bi^{4+\delta}$—O pair. Our results then imply that as Pb is doped into the material, the proportion of $Bi^{IV+\delta}$ increases, at the expense of the $Bi^{IV-\delta}$ states. On average the Bi valency is migrating towards a more 'Bi^{V}-like' state. This is perhaps not unexpected, as introduction of Pb into the material is effectively hole doping. As Pb in this material is in a Pb^{IV} state,[11,29] and oxygen deficiency in the material is not sufficient to compensate the introduced dopant,[42,43] some effective oxidation of Bi must occur on doping. The hypothesis that the average valence state of Bi increases on Pb doping is consistent with our previous XAS measurements of Bi L_{III} near-edge structure in this system.[29] More recently, these measurements have been repeated at substantially better resolution by

Hashimoto *et al.*, giving results in substantial agreement with this work.[43] In particular, these authors observe decreasing occupancy of the Bi 6s level (as evidenced by the increasing intensity of the pre-edge feature due to the $2p_{3/2,1/2} \rightarrow 6s$ transition) in the range $x = 1–0.2$.[43] Thus our EXAFS data is consistent with charge disproportion into $Bi^{IV+\delta}$ and $Bi^{IV-\delta}$ in $BaBiO_3$. Moreover, this is retained in the Pb-doped regime, with the dominant valence state becoming $Bi^{IV+\delta}$ as the Pb doping level increases.

Conclusions

EXAFS may be powerfully employed to observe the small structural variations which occur when a dopant is introduced into a well characterised oxide parent material, such as $SrSnO_3$. In addition, analysis of EXAFS data gives some information, from variations in bond lengths with doping, regarding the valency of the dopant. Here EXAFS shows that Sb dopes into $SrSnO_3$ as Sb^V, whilst two different sites (which we assign as '$Bi^{IV+\delta}$' and '$Bi^{IV-\delta}$') are observed for Bi in $BaBiO_3$. As Pb is doped into the material, the proportion of Bi in the $Bi^{IV+\delta}$ state increases progressively. The disproportionation, which is seen for the bismuthate but not the stannate, may be regarded as an instance of increasing lone-pair stability as the group is descended.

This work was funded by EPSRC. We thank Professor D. G. Nicholson for a number of useful discussions.

References

1 H. R. Aghabozorg, B. H. Sakakini, A. J. Roberts, J. C. Vickerman and W. R. Flavell, *Catal. Lett.* 1996, **39**, 97.

2 A. W. Sleight, J. L. Gillson and B. E. Bierstedt, *Solid State Commun.*, 1975, **17**, 27.

3 Y. Khan, K. Nahm, M. Rosenberg and H. Willner, *Phys. Status Solidi A*, 1977, **39**, 79.

4 A. J. Roberts, W. R. Flavell, D. R. C. Hoad, R. G. Egdell, S. Randall, P. L. Wincott and D. Teehan, *Surf. Sci.*, 1994, **311**, 181.

5 A. J. Roberts, PhD Thesis, UMIST, 1995.

6 R. G. Egdell, W. R. Flavell and P. J. Tavener, *J. Solid State Chem.*, 1984, **51**, 345.

7 W. R. Flavell, M. Mian, B. C. Morris, P. L. Wincott, D. Teehan and D. S.-L. Law, *Phys. Rev. B*, 1994, **49**, 595.

8 W. R. Flavell, D. R. C. Hoad, M. Mian, B. C. Morris, A. J. Roberts, M. M. Sarker, P. L. Wincott, D. Teehan and P. Bailey, *Surf. Sci.*, 1994, **307/308**, 1166.

9 R. J. Cava, P. Gammel, B. Batlogg, J. J. Krajewski, W. F. Peck, L. W. Rupp, R. Felder and R. B. van Dover, *Phys. Rev. B*, 1990, **42**, 4815.

10 J. B. Boyce, F. G. Bridges, T. Claeson, T. H. Geballe, G. G. Li and A. W. Sleight, *Phys. Rev. B*, 1991, **44**, 6961.

11 Z. Akhtar, M. J. Akhtar and C. R. A. Catlow, *J. Mater. Chem.*, 1994, **4**, 1081.

12 C. L. Lau and G. K. Wertheim, *J. Vac. Sci. Technol.*, 1978, **15**, 622.

13 S. M. Fray and J. T. S. Irvine, poster presentation at *Solid State Chemistry and Superconductivity Conference*, Aberdeen, 15th–17th July 1992.

14 C. Greaves, personal communication, 1991; S. M. A. Katib, MSc Thesis, University of Birmingham, 1986.

15 SERC Daresbury Laboratory EXCALIB and EXBACK programs, N. Binstead, J. W. Campbell, S. J. Gurman and P. C. Stephenson, 1990.

16 SERC Daresbury Laboratory EXCURV92 program, N. Binstead, J. W. Campbell, S. J. Gurman and P. C. Stephenson, 1991.

17 H. D. Megaw, *Proc. Phys. Soc.*, 1946, **58**, 10.

18 A. Vegas, M. Vallet-Regi, J. M. Gonzalez-Calbet and M. A. Alario-Franco, *Acta Crystallogr., Sect. B*, 1986, **42**, 167.

19 D. G. Nicholson, personal communication, 1994.

20 H. Y. P. Yong, *Acta Crystallogr., Sect. B*, 1974, **30**, 945.

21 C. Svensson, *Acta Crystallogr., Sect. B*, 1974, **30**, 458.

22 C. Chaillout, A. Santoro, J. P. Remeika, A. S. Cooper, G. P. Espinosa and N. Marezio, *Solid State Commun.*, 1988, **65**, 1363.

23 R. Claessen, M. G. Smith, J. B. Goodenough and J. W. Allen, *Phys. Rev. B*, 1993, **47**, 1788.

24 J. Amador, E. G. Puebla, M. A. Monge, I. Rasines and C. R. Valero, *Inorg. Chem.*, 1988, **27**, 1367.

25 R. G. Egdell, S. Eriksen and W. R. Flavell, *Surf. Sci.*, 1987, **192**, 265.

26 R. G. Egdell, in *Science of Ceramic Interfaces II*, ed. J. Nowotny, Elsevier, Amsterdam, 1994, p. 527.

27 P. A. Lee, P. H. Citrin, P. Eisenberger and B. M. Kincaid, *Rev. Mod. Phys.*, 1981, **53**, 769.

28 D. J. Singh, D. A. Papaconstantopoulos, J. P. Julien and F. Cyrot-Lackmann, *Phys. Rev. B*, 1991, **44**, 9519.

29 W. R. Flavell, B. C. Morris, I. Tweddell, D. Purdie, G. Thornton, P. L. Wincott and R. L. Bilsborrow, *J. Mater. Chem.*, 1992, **2**, 1209.

30 T. K. Sham, *Phys. Rev. B*, 1985, **31**, 1888.

31 D. E. Cox and A. W. Sleight, *Solid State Commun.*, 1976, **19**, 969.

32 G. Thornton and A. J. Jacobson, *Acta Crystallogr., Sect. B*, 1978, **34**, 351.

33 J. B. Boyce, F. G. Bridges, T. Claeson, T. H. Geballe and J. M. Remeika, *Phys. Rev. B*, 1990, **41**, 6306.

34 D. T. Marx, P. G. Radaelli, J. D. Jorgensen, R. L. Hitterman, D. G. Hinks, S. Pei and B. Dabrowski, *Phys. Rev. B*, 1992, **46**, 1144.

35 A. F. Orchard and G. Thornton, *J. Chem. Soc., Dalton Trans.*, 1977, 1238.

36 G. U. Kulkarni, V. Vijayakrishnan, G. Ranga Rao, Ram Seshadri and C. N. R. Rao, *Appl. Phys. Lett.*, 1990, **57**, 1823.

37 A. Winiarski, G. Wübbeler, Chr Scharfschwerdt, E. Clausing and M. Neumann, *Fresenius J. Anal. Chem.*, 1991, **341**, 296.

38 G. K. Wertheim, J. P. Remeika and D. N. E. Buchanan, *Phys. Rev. B*, 1982, **26**, 2120.

39 Z-X. Shen, P. A. P. Lindberg, B. O. Wells, D. S. Dessau, A. Borg, I. Lindau, W. E. Spicer, W. P. Ellis, G. H. Kwei, K. C. Ott, J-S. Kang and J. W. Allen, *Phys. Rev. B*, 1989, **40**, 6912.

40 H. Guyot, Cl Filippini and J. Marcus, *J. Alloys Compds.*, 1993, **195**, 543.

41 M. Nagoshi, T. Suzuki, Y. Fukuda, A. Tokiwa-Yamamoto, Y. Syono and M. Tachiki, *Phys. Rev. B*, 1993, **47**, 5196.

42 T. Hashimoto and H. Kawazoe, *Solid State Commun.*, 1993, **87**, 251.

43 T. Hashimoto, H. Kawazoe and H. Shimamura, *Physica C*, 1994, **223**, 131.

Paper 6/04959A; *Received* 15*th July*, 1996